

Roller Racer with Varying Gyrostatic Momentum: Acceleration Criterion and Strange Attractors

Ivan A. Bizyaev^{1*} and Ivan S. Mamaev^{2**}

¹*Ural Mathematical Center, Udmurt State University,
ul. Universitetskaya 1, 426034 Izhevsk, Russia*

²*Kalashnikov Izhevsk State Technical University,
ul. Studencheskaya 7, 426069 Izhevsk, Russia*

Received November 07, 2022; revised December 21, 2022; accepted December 27, 2022

Abstract—In this paper we investigate a nonholonomic system with parametric excitation, a Roller Racer with variable gyrostatic momentum. We examine in detail the problem of the existence of regimes with unbounded growth of energy (nonconservative Fermi acceleration). We find a criterion for the existence of trajectories for which one of the velocity components increases without bound and has asymptotics $t^{1/3}$. In addition, we show that the problem under consideration reduces to analysis of a three-dimensional Poincaré map. This map exhibits both regular attractors (a fixed point, a limit cycle and a torus) and strange attractors.

MSC2010 numbers: 37J60, 34A34

DOI: 10.1134/S1560354723010070

Keywords: nonholonomic mechanics, Roller Racer, Andronov–Hopf bifurcation, stability, central manifold, unbounded speedup, Poincaré map, limit cycle, strange attractor

Contents

1	INTRODUCTION	108
2	EQUATIONS OF MOTION	109
3	INERTIAL MOTION: THE ANDRONOV–HOPF BIFURCATION	114
4	CRITERION FOR ACCELERATION OF A ROLLER RACER WITH PERIODIC EXCITATION	118
5	NUMERICAL INVESTIGATIONS OF THE POINCARÉ MAP	123
	ACKNOWLEDGMENTS	128
	FUNDING	128
	CONFLICT OF INTEREST	128
	REFERENCES	128

*E-mail: bizyaevtheory@gmail.com

**E-mail: mamaev@rcd.ru

1. INTRODUCTION

This paper continues a series of studies on the dynamics of various wheeled vehicles [3–7, 9, 10, 12, 13, 29, 34, 36, 37]. We will not review here in detail the existing literature on this topic. A more detailed review can be found in [7, 10, 29].

We especially note the papers [4, 6–8], in which an unusual dynamical phenomenon is revealed, namely, nonlinear nonholonomic acceleration under the action of bounded periodic excitation generated by the prescribed motion of structural elements (point masses, rotors, etc.). This phenomenon has a certain similarity to Fermi acceleration [18], which is observed in celestial mechanics systems and billiards (see [7] for details). In the papers [4, 6–8], for the *simplest wheeled system*, the Chaplygin sleigh (or, which is the same, a two-wheeled platform) it is rigorously shown that for accelerating trajectories, depending on the choice of change in the mass distribution, the translational velocity of the sleigh has the asymptotics of growth $t^{\frac{1}{2}}$ or $t^{\frac{1}{3}}$. In addition, for accelerating trajectories the sleigh moves on average along some straight line. As is well known, the simplicity of the system considered (the Chaplygin sleigh) has the result that, whereas its theoretical analysis is much simpler, it is fairly difficult to implement such a design in practice.



Fig. 1.

For this reason, the problem of finding nonlinear nonholonomic acceleration in wheeled systems which could be implemented in practice remained unsolved.

In this paper, we consider the design of a wheeled vehicle consisting of two platforms connected to each other, with rigidly attached wheel pairs. Such a design is implemented, for example, in various child vehicles such as the *Roller Racer* and the *twistcar* (see Fig. 1). The inertial motion of such systems is examined in [3, 13].

A distinctive feature of the Roller Racer and the twistcar is that a child can move ahead by periodic oscillations of the handlebar in the transverse direction. The dynamics of such systems under the assumption that the angle between the platforms is a given periodic function of time is considered in [5, 15, 29, 36]. It turns out that in this case the wheeled vehicle speeds up indefinitely and its translational velocity increases linearly with time t . Nonetheless, the wheeled vehicle does not always move on average along a straight line. For example, when some velocity is reached, it can turn around and start moving in the opposite direction [5].

In this paper it is assumed that each of the two platforms has a rotor whose angular velocity is a given periodic function of time. It is shown that in this case it is possible to achieve an acceleration where the velocity of the system increases as $t^{1/3}$ and the device moves in a strip bounded by two straight lines (see Section 4, in which the acceleration criterion is stated).

The system considered in this paper reduces to analysis of a three-dimensional Poincaré map (that possesses no invariant measure) on a noncompact manifold. A qualitative description of various bifurcations encountered in such systems is given, for example, in [22, 24, 25, 43]. In this paper we consider the case in which this Poincaré map possesses an involution and in which, for a sufficiently small amplitude of the gyrostatic momentum, the map exhibits only asymptotically stable and asymptotically unstable equilibrium points symmetric to them. As the gyrostatic momentum increases, these equilibria undergo bifurcations resulting in a strange attractor and a strange repeller, which can occupy a rather large area in the map, and thus an intersection of

their closures arises, which leads to extremely complex behavior of the system, which was called *mixed dynamics*¹⁾ [20, 27]. Although the term *mixed dynamics* has appeared only relatively recently, there has been quite a lot of research into models in which mixed dynamics is observed (see, e.g., [1, 17, 32, 33]).

We also note that dynamical systems arising in nonholonomic mechanics are also of interest from a theoretical point of view since they can exhibit a variety of phenomena. For example, the dynamics of more complex modifications of a wheeled vehicle with a rotor has been examined previously, namely, that of a *snakeboard* [9, 37, 40] and that of a *skateboard* [31], each of which is a platform to which two moving wheel pairs are fastened. The rolling of a sphere with periodically varying mass distribution was investigated in [2, 34, 39].

We note that this work allows formulation of some natural problems relating to the dynamics of the Roller Racer. Specifically, the question of the possibility of acceleration with the velocity increasing as $t^{1/2}$ remains unsolved. The problem of analyzing the form of the trajectories of the Roller Racer depending on solutions to the reduced system (reconstruction of dynamics) also remains beyond the scope of this paper.

Another interesting unsolved problem is to find an explicit criterion of nonholonomic nonlinear acceleration for spherical robots for which the existence of acceleration was established only numerically [34].

2. EQUATIONS OF MOTION

Schematic design and basic assumptions. Consider a Roller Racer moving on a horizontal plane (see Fig. 2). For this Roller Racer we assume the following natural assumptions to be satisfied which allow us to formulate mathematical model of the system.

- A1.** Two platforms are connected to each other by means of a joint at point P so that they can rotate freely about the vertical axis.
- A2.** Each platform has a balanced rotor with a vertical axis of rotation. In what follows, we will assume that the angular velocity of each rotor is a given (periodic) function of time.
- A3.** A wheel pair is rigidly attached to each platform. Both wheel pairs are balanced so that their center of mass is in the middle of the axis connecting the wheels.
- A4.** Each wheel rolls with one point in contact with the supporting plane, and there is no slipping.

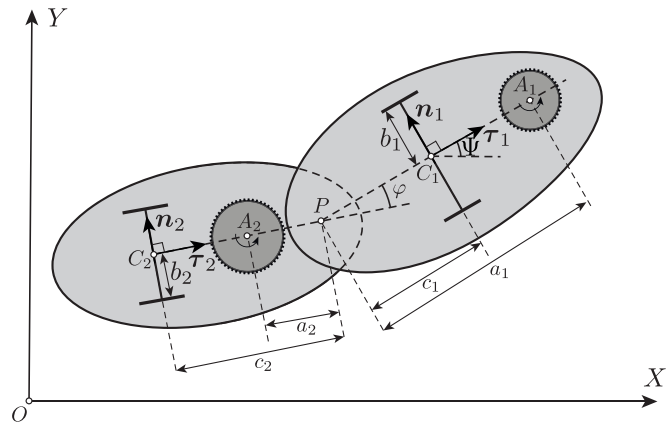


Fig. 2. Possible scheme of a balanced Roller Racer with rotors on the plane (top view) satisfying the condition of balance of PC_1 and PC_2 , which are perpendicular to the axes of the wheel pairs; A_1 and A_2 are the position of the modified center of mass of the platform in which the axes of the rotors are fastened.

¹⁾The term *mixed dynamics* was coined in the paper [19]

According to [10], *wheel-knife equivalence* takes place in this case: any wheel can be replaced with an equivalent knife edge which also moves with one point in contact with the support (this point coincides with the point of contact of the wheel), and the velocity of the platform at the point of contact in the direction perpendicular to the plane of the knife edge vanishes. In this case, the mass of the knife edge is calculated by the formula

$$m_s = m_w + \frac{i_w}{d_w^2}, \quad (2.1)$$

where m_w , d_w , i_w are the mass, the radius and the axial moment of inertia of the corresponding wheel, respectively. The moment of inertia of the knife edge relative to the vertical axis passing through the point of contact coincides with the moment of inertia of the corresponding wheel:

$$j_s = j_w. \quad (2.2)$$

Using the wheel-knife equivalence, we replace all wheels with corresponding knife edges and define the centers of mass for each of the resulting platforms taking into account the attached knife edges and rotors, and denote the corresponding modified centers of mass by A_1 and A_2 . In addition, we make an additional assumption that the platforms are balanced.

A5. The modified center of mass of each platform A_k , $k = 1, 2$ is on the straight line PC_k passing through the point of connection P and perpendicular to the axis of the corresponding wheel pair.

Configuration space and constraints. We define a fixed (inertial) coordinate system OXY . Let $\mathbf{r} = (X, Y)$ be the radius vector of the point of connection of the platforms P . Let us specify the orientation of the first platform by angle Ψ between the axis Ox and the straight line PA_1 , and the orientation of the second platform by angle φ between the straight lines PA_1 and PA_2 .

Here we use again the wheel-knife equivalence and exclude from consideration the angles of rotation of the wheels about the axes of the corresponding wheel pairs. Thus, the configuration space of the platforms \mathcal{N}^4 is the following four-dimensional manifold:

$$\mathcal{N}^4 = \{\mathbf{q} = (X, Y, \Psi, \varphi) \mid \Psi, \varphi \bmod 2\pi\} \simeq \mathbb{R}^2 \times \mathbb{T}^2.$$

Now we define the unit vectors directed along the normal to the plane of the wheels for the first and the second platform (see Fig. 2). Referred to the axes OXY , they have the form

$$\mathbf{n}_1 = (-\sin \Psi, \cos \Psi), \quad \mathbf{n}_2 = (-\sin(\Psi + \varphi), \cos(\Psi + \varphi)).$$

The condition that there be no slipping of the points of contact of the wheels in the direction \mathbf{n}_1 and \mathbf{n}_2 defines the required constraints:

$$f_1 = (\dot{\mathbf{r}}, \mathbf{n}_1) + c_1 \dot{\Psi} = 0, \quad f_2 = (\dot{\mathbf{r}}, \mathbf{n}_2) - c_2 (\dot{\Psi} + \dot{\varphi}) = 0. \quad (2.3)$$

Kinetic energy. Using relations (2.1) and (2.2), we can represent the kinetic energy of the system as

$$T = T^{(2)} + T^{(1)},$$

where $T^{(2)}$ and $T^{(1)}$ are terms which depend quadratically and linearly on the generalized velocities $\dot{X}, \dot{Y}, \dot{\Psi}$ and $\dot{\varphi}$:

$$\begin{aligned} T^{(2)} &= \frac{m_1}{2} (\dot{\mathbf{r}} + a_1 \dot{\Psi} \mathbf{n}_1)^2 + \frac{I_1}{2} \dot{\Psi}^2 + \frac{m_2}{2} (\dot{\mathbf{r}} - a_2 (\dot{\Psi} + \dot{\varphi}) \mathbf{n}_2)^2 + \frac{I_2}{2} (\dot{\Psi} + \dot{\varphi})^2, \\ T^{(1)} &= k_1(t) \dot{\Psi} + k_2(t) (\dot{\Psi} + \dot{\varphi}), \end{aligned} \quad (2.4)$$

$$m_\alpha = m_0^{(\alpha)} + m_r^{(\alpha)} + 2 \left(m_w^{(\alpha)} + \frac{i_w^{(\alpha)}}{(d_w^{(\alpha)})^2} \right),$$

$$I_\alpha = I_0^{(\alpha)} + I_r^{(\alpha)} + \sum_{\beta=1}^2 \left(j_w^{(\alpha)} + \left(m_w^{(\alpha)} + \frac{i_w^{(\alpha)}}{(d_w^{(\alpha)})^2} \right) (r_w^{(\alpha\beta)})^2 \right),$$

$$k_\alpha(t) = i_r^{(\alpha)} \omega_\alpha(t), \quad \alpha = 1, 2,$$

where $k_1(t), k_2(t)$ are the gyrostatic moments arising due to a given rotation of the rotors. The parameters of the model are given in Table 1.

If the modified center of mass of the α th platform A_α and the center of mass of the corresponding wheel pair C_α lie on different sides of the point of connection of the platforms, P , then in the kinetic energy (2.4) one needs to make the change of variables $a_\alpha \rightarrow -a_\alpha$. In order to take this case into consideration, we will assume that the *parameters a_1 and a_2 can take negative values*.

Natural quasi-velocities. As demonstrated in [12], the analysis of the dynamics of nonholonomic systems simplifies considerably if one chooses appropriate quasi-velocities (i.e., a special parameterization of the generalized velocities of the system). Specifically, in this case we choose quasi-velocities u, v, w_1 and w_2 which satisfy the following conditions:

- the functions u, v, w_1 and w_2 do not vary after changing the fixed coordinate system OXY , i.e., *they are invariants of the group of motions of the plane $SE(2)$* ;
- the constraint Eqs. (2.3) are represented as

$$w_1 = 0, \quad w_2 = 0, \quad (2.5)$$

i. e., *we choose a natural basis of quasi-velocities* [12];

- the quadratic part $T^{(2)}$ of the kinetic energy (2.4) restricted to the constraints turns out to be a diagonal quadratic form in u and v .

Table 1. Parameters of the model

Parameter	Definition
$\alpha = 1, 2$	the number of the platform
$m_0^{(\alpha)}$	the unladen weight of the platform (without wheels and rotor)
$I_0^{(\alpha)}$	the intrinsic moment of inertia of the platform relative to the point of connection P
$m_r^{(\alpha)}$	the mass of the rotor
$I_r^{(\alpha)}$	the moment of inertia of the rotor relative to point P
$i_r^{(\alpha)}$	the moment of inertia of the rotor relative to the axis of rotation
$m_w^{(\alpha)}$	the mass of the wheel
$d_w^{(\alpha)}$	the radius of the wheel
$i_w^{(\alpha)}$	the moment of inertia of the wheel relative to the axis of rotation
$j_w^{(\alpha)}$	the moment of inertia of the wheel relative to the vertical axis passing through the point of contact
$r_w^{(\alpha\beta)} \beta = 1, 2$	the distance from point P to the point of contact of the β th wheel with the support
a_α	the distance from point P to the modified center of mass A_α
c_α	the distance from point P to the axis of the wheel pair

Furthermore, we assume that the distances from point P to the wheel pairs of each of the platforms are different, i. e., $c_1 \neq c_2$. Without loss of generality we also assume that

$$c_1 > c_2 > 0. \quad (2.6)$$

The corresponding quasi-velocities are given by the relations

$$\begin{aligned} w_1 &= \frac{1}{c_2}(\dot{\mathbf{r}}, \mathbf{n}_1) + \frac{c_1}{c_2}\dot{\Psi}, \quad w_2 = \frac{1}{c_1}(\dot{\mathbf{r}}, \mathbf{n}_2) - \frac{c_2}{c_1}(\dot{\Psi} + \dot{\varphi}), \quad u = \frac{\sqrt{\Phi(\varphi)}}{\sqrt{J(\varphi)}}\dot{\varphi}, \\ v &= \frac{1}{(A - B)\sqrt{J(\varphi)}} \left[(m_1 + m_2)(\dot{\mathbf{r}}, c_1\boldsymbol{\tau}_2 + c_2\boldsymbol{\tau}_1) + G(\boldsymbol{\tau}_1, \mathbf{n}_2)\dot{\Psi} - D(\boldsymbol{\tau}_2, \mathbf{n}_1)(\dot{\Psi} + \dot{\varphi}) \right. \\ &\quad \left. + \frac{AB}{c_1 - c_2}((\dot{\mathbf{r}}, \mathbf{n}_1 + \mathbf{n}_2) + c_1\dot{\Psi} - c_2(\dot{\Psi} + \dot{\varphi})) \right], \\ \boldsymbol{\tau}_1 &= (\cos \Psi, \sin \Psi), \quad \boldsymbol{\tau}_2 = (\cos(\Psi + \varphi), \sin(\Psi + \varphi)), \end{aligned} \quad (2.7)$$

where the following functions and parameters have been introduced:

$$\begin{aligned} J_1(\varphi) &= A^2 + G \sin^2 \varphi - AB \cos \varphi, \quad J_2(\varphi) = B^2 + D \sin^2 \varphi - AB \cos \varphi, \\ J(\varphi) &= J_1(\varphi) + J_2(\varphi) > 0, \quad \Phi(\varphi) = \frac{(A^2 + G)(B^2 + D)}{(A - B)^2} - \frac{GD}{(A - B)^2} \cos^2 \varphi > 0, \\ A &= c_1\sqrt{m_1 + m_2}, \quad B = c_2\sqrt{m_1 + m_2}, \\ G &= I_1 + m_1((a_1 - c_1)^2 - c_1^2), \quad D = I_2 + m_2((a_2 - c_2)^2 - c_2^2). \end{aligned} \quad (2.8)$$

By virtue of assumption (2.6), the inequality $A > B$ holds.

Remark 1. The conditions formulated above do not uniquely define the quasi-velocities u , v , w_1 and w_2 .

Remark 2. Generally speaking, the parameters G and D can become negative if most of the mass of each platform is concentrated near point P .

As can be seen, the variables w_1 , w_2 , v and u have the dimension of angular velocities. In these variables, the constraint equations (2.3) look particularly simple:

$$w_1 = 0, \quad w_2 = 0. \quad (2.9)$$

Moreover, if one ignores the terms quadratic in w_1 and w_2 (since, by virtue of (2.9), they make no contribution to the equations of motion [10]) $T^{(2)}$ can be represented as

$$\begin{aligned} T^{(2)} &= \frac{(A - B)^2}{2}(v^2 + u^2) - \frac{v \sin \varphi}{\sqrt{J(\varphi)}} \left(\Delta(A - B)w_1 + (A^2B - \Gamma(A - B))(w_1 + w_2) \right) \\ &\quad - \frac{u}{\sqrt{J(\varphi)\Phi(\varphi)}} \left(\Delta J_2(\varphi)w_1 - \Gamma(J_2(\varphi)w_1 - J_1(\varphi)w_2) \right. \\ &\quad \left. - (Aw_2 - Bw_1 \cos \varphi)(B(A^2 + G) - AD \cos \varphi) \right) + O(w_1^2) + O(w_2^2), \\ \Gamma &= m_2a_2c_1, \quad \Delta = \left(\left(\frac{a_1}{c_1} - 1 \right) m_1 + \left(\frac{a_2}{c_2} - 1 \right) m_2 \right) c_1c_2. \end{aligned} \quad (2.10)$$

As can be seen, after restriction to the constraints (2.9) the preceding expression does not depend explicitly on φ :

$$(T^{(2)})^* = \frac{(A - B)^2}{2}(v^2 + u^2), \quad (2.11)$$

where $(\)^*$ denotes the restriction to the constraints (2.9).

After solving relations (2.7), we obtain a representation for the generalized velocities in the form

$$\dot{\mathbf{q}} = v\mathbf{E}_1 + u\mathbf{E}_2 + w_1\boldsymbol{\Sigma}_1 + w_2\boldsymbol{\Sigma}_2, \quad (2.12)$$

where the vector fields \mathbf{E}_1 and \mathbf{E}_2 form a basis of distribution in the tangent bundle of the configuration space \mathcal{N}^4 , which is given by the constraints (2.3), and the vector fields $\boldsymbol{\Sigma}_1$, $\boldsymbol{\Sigma}_2$ are transversal to this distribution. Moreover, to derive the equations of motion we need the commutator of the vector fields \mathbf{E}_1 and \mathbf{E}_2 , for which the following relation holds:

$$[\mathbf{E}_1, \mathbf{E}_2] = \frac{(A - B)}{\sqrt{\Phi(\varphi)}} (\boldsymbol{\Sigma}_2 - \boldsymbol{\Sigma}_1).$$

Remark 3. We do not present here the explicit form of the vector fields \mathbf{E}_1 , \mathbf{E}_2 , $\boldsymbol{\Sigma}_1$, $\boldsymbol{\Sigma}_2$ due to their cumbersome form. Instead, we present a step-by-step algorithm for deriving the equations of motion, which will allow us to verify the relations presented here. In addition, the vector fields \mathbf{E}_1 and \mathbf{E}_2 are, generally speaking, contained in Eqs. (2.14) and (2.16), which are presented below and govern the evolution of the variables X , Y , Ψ and φ in terms of the quasi-velocities v and u .

Equations of motion, reduction and reconstruction. In order to obtain equations of motion in the chosen quasi-velocities (2.7), we make use of the results of [12]. We also note that the kinetic energy consists of two terms $T^{(2)}$ and $T^{(1)}$, and in this case it is convenient to calculate the contribution of each of these terms in the equations of motion by different methods. Specifically, we represent the equations of motion as

$$\begin{aligned} \frac{d}{dt} \left(\frac{\partial(T^{(2)})^*}{\partial v} \right) &= \frac{(A - B)u}{\sqrt{\Phi(\varphi)}} \left(\left(\frac{\partial T^{(2)}}{\partial w_1} \right)^* - \left(\frac{\partial T^{(2)}}{\partial w_2} \right)^* \right) + (\mathbf{Q}, \mathbf{E}_1), \\ \frac{d}{dt} \left(\frac{\partial(T^{(2)})^*}{\partial u} \right) &= -\frac{(A - B)v}{\sqrt{\Phi(\varphi)}} \left(\left(\frac{\partial T^{(2)}}{\partial w_1} \right)^* - \left(\frac{\partial T^{(2)}}{\partial w_2} \right)^* \right) + (\mathbf{Q}, \mathbf{E}_2). \\ \mathbf{Q}(t) &= -\frac{d}{dt} \left(\frac{\partial T^{(1)}}{\partial \dot{\mathbf{q}}} \right) + \frac{\partial T^{(1)}}{\partial \mathbf{q}} = (0, 0, -\dot{k}_1(t) - \dot{k}_2(t), -\dot{k}_2(t)). \end{aligned} \quad (2.13)$$

Such a representation allows us to obtain in a natural way the equations solved for the derivatives \dot{u} and \dot{v} .

Substituting relations (2.10) and (2.11), we obtain the reduced equations of motion governing the evolution of the variables u , v and φ :

$$\begin{aligned} \frac{dv}{dt} &= uW + \sin \varphi f(t, \varphi), \quad \frac{du}{dt} = -vW + g(t, \varphi), \quad \frac{d\varphi}{dt} = \frac{\sqrt{J(\varphi)}}{\sqrt{\Phi(\varphi)}} u, \\ W &= \frac{\sin \varphi \Delta v}{\sqrt{J(\varphi)\Phi(\varphi)}} - \frac{Z(\varphi)u}{\Phi(\varphi)\sqrt{J(\varphi)}}, \end{aligned} \quad (2.14)$$

where the following functions have been introduced:

$$\begin{aligned} f(t, \varphi) &= \frac{\dot{k}_1 + \dot{k}_2}{(A - B)\sqrt{J(\varphi)}}, \quad g(t, \varphi) = \frac{J_2(\varphi)\dot{k}_1(t) - J_1(\varphi)\dot{k}_2(t)}{(A - B)^2\sqrt{J(\varphi)\Phi(\varphi)}}, \\ Z(\varphi) &= \frac{DJ_1(\varphi) - GJ_2(\varphi)}{A - B} \cos \varphi + \frac{\Gamma - AB}{A - B} J_1(\varphi) + \frac{\Gamma - \Delta}{A - B} J_2(\varphi). \end{aligned} \quad (2.15)$$

Thus, as a result of the use of the quasi-velocities satisfying the above-mentioned conditions, at the first stage the problem boils down to investigating the nonautonomous reduced system (2.14) on

$$\mathcal{M}_r^3 = \{(v, u, \varphi)\} \simeq \mathbb{R}^2 \times \mathbb{S}^1.$$

From the known solutions of the reduced system (2.14), the behavior of the configuration variables is described, according to (2.7), by the relations (reconstruction of dynamics):

$$\begin{aligned} \frac{d\Psi}{dt} &= -v \frac{A-B}{\sqrt{J(\varphi)}} \sin \varphi - u \frac{J_2(\varphi)}{\sqrt{J(\varphi)\Phi(\varphi)}}, \\ \frac{dX}{dt} &= \frac{vc_2(A-B)}{B\sqrt{J(\varphi)}} (A \cos(\varphi + \Psi) + B \cos \Psi) \\ &- \frac{uc_2}{B\sqrt{J(\varphi)\Phi(\varphi)}} (AJ_2(\varphi) \sin \Psi + (B(A^2 + G) - AD \cos \varphi) \sin \varphi \cos \Psi), \\ \frac{dY}{dt} &= \frac{vc_2(A-B)}{B\sqrt{J(\varphi)}} (A \sin(\varphi + \Psi) + B \sin \Psi) \\ &+ \frac{uc_2}{B\sqrt{J(\varphi)\Phi(\varphi)}} (AJ_2(\varphi) \cos \Psi - (B(A^2 + G) - AD \cos \varphi) \sin \varphi \sin \Psi). \end{aligned} \quad (2.16)$$

Next, we analyze how the presence of varying gyrostatic momenta $k_1(t)$, $k_2(t)$ affects the dynamics of the wheeled vehicle. Specifically, of particular interest is the question whether the system (2.14) has unbounded trajectories on the plane $\mathbb{R}_{v,u}^2 = \{(v, u)\}$. For them, the velocity of the platforms, and hence their kinetic energy, must indefinitely increase (in absolute value) in the course of time.

Remark 4. As can be seen, the reduced system (2.14) depends only on six parameters $A, B, G, D, \Delta, \Gamma$, which are expressed using (2.8) and (2.10) in terms of eight initial parameters of the problem $m_i, I_i, a_i, c_i, i = 1, 2$. The region of physically admissible values of these six parameters must be chosen in such a way that the relations $m_i > 0$ and $I_i > 0$ are satisfied and that these relations can be reduced to the inequalities

$$\begin{aligned} I_1 &= G + A^2 - \frac{(\Delta - \Gamma)^2}{B^2} - \frac{(AB + \Delta - \Gamma)^2}{B^2} \frac{m_2}{m_1} > 0, \\ I_2 &= D + \frac{2\Gamma B - \Gamma^2}{A} - \frac{\Gamma^2}{A^2} \frac{m_1}{m_2} > 0, \quad m_1 > 0, \quad m_2 > 0. \end{aligned} \quad (2.17)$$

3. INERTIAL MOTION: THE ANDRONOV–HOPF BIFURCATION

Suppose that there are no gyrostatic momenta ($k_1 = 0$, $k_2 = 0$). Then the problem reduces to investigating the inertial motion of the Roller Racer ($\mathbf{Q} = 0$). Under these assumptions the system (2.14) possesses the energy integral

$$E = \frac{(A-B)^2}{2}(v^2 + u^2). \quad (3.1)$$

The fixed level of energy in the phase space \mathcal{M}_r^3 of the reduced system (2.14) is a two-dimensional torus

$$\mathcal{M}_h^2 = \{(v, u, \varphi) \mid E(v, u) = h(A-B)^2\} \simeq \mathbb{T}^2.$$

Remark 5. As can be seen, only the time derivatives of the gyrostatic momentum appear in the equations of motion (2.14). Therefore, if $k_1(t)$ and $k_2(t)$ are constants, then the equations of motion are identical to the equations of a wheeled vehicle without rotors. This is due to the fact that the function $T^{(1)}$ for constant gyrostatic momentum reduces to the total derivative with respect to the generalized coordinates φ and ψ and therefore makes no contribution to the equations of motion.

The system (2.14) is invariant under the transformation

$$v \rightarrow Cv, \quad u \rightarrow Cu, \quad t \rightarrow \frac{t}{C} \quad C = \text{const.} \quad (3.2)$$

In that process, the value of the energy integral h is transformed as

$$h \rightarrow C^2 h.$$

Thus, we obtain the following statement.

Proposition 1. Let $k_1 = k_2 = 0$, then the trajectories of the reduced system (2.14) on different level sets of the energy integral \mathcal{M}_h^2 (except for $h = 0$) are identical up to the transformation (3.2).

Consequently, it suffices to consider the trajectories of the system (2.14) on one fixed level of energy \mathcal{M}_h^2 . To do so, we define the angle variable ϑ :

$$v = \sqrt{2h} \sin \vartheta, \quad u = \sqrt{2h} \cos \vartheta.$$

This gives us a system on the torus \mathbb{T}^2 whose trajectories in the angle variables $\mathbf{x} = (\varphi, \vartheta) \bmod 2\pi$ are given by the equations

$$\begin{aligned} \frac{d\varphi}{dt} &= \frac{\sqrt{2h}}{\sqrt{\Phi(\varphi)}} \sqrt{J(\varphi)} \cos \vartheta, \\ \frac{d\vartheta}{dt} &= \frac{\sqrt{2h}}{\Phi(\varphi) \sqrt{J(\varphi)}} (\Delta \sin \vartheta \sin \varphi \sqrt{\Phi(\varphi)} - \cos \vartheta Z(\varphi)). \end{aligned} \quad (3.3)$$

Since, according to (2.8), $J(\varphi)$, $\Phi(\varphi)$ and $Z(\varphi)$ are even functions, the system (3.3) possesses two involutions:

$$R^{(1)} : \varphi \rightarrow \varphi, \vartheta \rightarrow \vartheta + \pi, t \rightarrow -t,$$

$$R^{(2)} : \varphi \rightarrow -\varphi, \vartheta \rightarrow -\vartheta, t \rightarrow -t,$$

i.e., this system is reversible. Under the action of these transformations any trajectory of the system becomes a trajectory with an opposite direction of motion.

Relative equilibria. It can be shown that the system (3.3) always possesses only four isolated fixed points, which we divide into two groups, depending on the value of the angle φ .

1. Points $\mathbf{x}_0^{(+)} = \left(0, \frac{\pi}{2}\right)$ and $\mathbf{x}_0^{(-)} = \left(0, \frac{3\pi}{2}\right)$.

2. Points $\mathbf{x}_\pi^{(+)} = \left(\pi, \frac{\pi}{2}\right)$ and $\mathbf{x}_\pi^{(-)} = \left(\pi, \frac{3\pi}{2}\right)$.

For them, according to (2.16), we have $\psi = \text{const}$. Therefore, these fixed points correspond to the *motion of a wheeled vehicle in a straight line*. Note that for the first group the vectors τ_1 and τ_2 are codirectional, i.e., the platforms are “unfolded”, and for the second group the vectors τ_1 and τ_2 also lie on one straight line, but are directed in opposite directions, i.e., in this case, by contrast, the platforms are “folded up”, see Fig. 3.

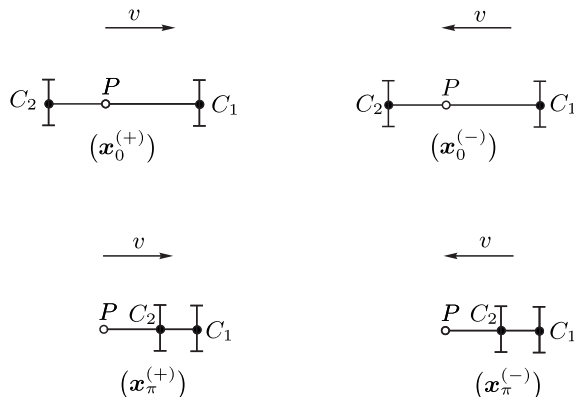


Fig. 3. Scheme of the motion of the Roller Racer for relative equilibria ($v = \pm\sqrt{2h}$, $u = 0$).

The characteristic polynomials for $\mathbf{x}_0^{(+)}$ and $\mathbf{x}_\pi^{(+)}$ have the form

$$\begin{aligned} p_0^{(+)}(\lambda) &= \lambda^2 + \frac{\sqrt{2h}(A-B)Q_0}{A^2B^2 + A^2D + B^2G}\lambda + \frac{2\Delta h(A-B)^2}{A^2B^2 + A^2D + B^2G}, \\ p_\pi^{(+)}(\lambda) &= \lambda^2 + \frac{\sqrt{2h}(A-B)Q_\pi}{A^2B^2 + A^2D + B^2G}\lambda - \frac{2\Delta h(A-B)^2}{A^2B^2 + A^2D + B^2G}, \\ Q_{0/\pi} &= A^2B \mp AD - A\Gamma \mp B\Delta - BG \pm B\Gamma, \end{aligned} \quad (3.4)$$

where the upper sign corresponds to Q_0 , and the lowe sign, to Q_π .

The other pair of fixed points can be obtained using the involution $R^{(1)}$:

$$R^{(1)} : x_0^{(+)} \rightarrow x_0^{(-)}, \quad R^{(1)} : x_\pi^{(+)} \rightarrow x_\pi^{(-)}.$$

As a consequence, the characteristic polynomials for $\mathbf{x}_0^{(-)}$ and $\mathbf{x}_\pi^{(-)}$ are defined, respectively, by the relations

$$p_0^{(-)}(\lambda) = p_0^{(+)}(-\lambda), \quad p_\pi^{(-)}(\lambda) = p_\pi^{(+)}(-\lambda). \quad (3.5)$$

Proposition 2. *If $\Delta \neq 0$, then the system (3.3) has four isolated fixed points. Among them, only one is asymptotically stable, and the other three are unstable.*

Proof. In this case, according to the Routh–Hurwitz criterion, a necessary and sufficient condition for a fixed point to be stable is that all coefficients of the characteristic polynomial be positive.

Since the sign of the free term in the polynomials (3.4) does not change under the transformation (3.5), we may conclude that, depending on the sign of the quantity

$$\tilde{\Delta} = \frac{\Delta}{A^2B^2 + A^2D + B^2G},$$

one of two pairs of the fixed points turns out to be unstable (more exactly, saddle) points:

- if $\tilde{\Delta} > 0$, then $\mathbf{x}_\pi^{(+)}$ and $\mathbf{x}_\pi^{(-)}$ are unstable;
- if $\tilde{\Delta} < 0$, then $\mathbf{x}_0^{(+)}$ and $\mathbf{x}_0^{(-)}$ are unstable.

On the other hand, the transformation (3.5) changes the sign of the coefficient with the term linear in λ in the characteristic polynomial. This implies that, if the free term is positive, then one of the points in the corresponding pair is stable and the other is unstable. \square

Remark 6. It follows from (3.3) that, for $\Delta = 0$, degenerate one-parameter families of fixed points arise in the system. This case is examined in detail in [3].

Qualitative analysis of the reduced system. We now consider the question of how the form of the phase portrait of the system (3.3) changes as the parameters are varied.

To do so, we fix all parameters and change only the parameter Γ , assuming that

$$\Delta > 0, \quad A^2B^2 + A^2D + B^2G > 0.$$

According to (3.4) and (3.5), the fixed points $\mathbf{x}_\pi^{(+)}$ and $\mathbf{x}_\pi^{(-)}$ are always saddles.

Consequently, the equilibrium points $\mathbf{x}_0^{(+)}$ and $\mathbf{x}_0^{(-)}$ are simultaneously either nodes or foci, depending on the quantity

$$\mathcal{D}_0 = Q_0^2 - 4\Delta(A^2B^2 + A^2D + B^2G),$$

which is proportional to the discriminant of the characteristic polynomials $p_0^{(+)}(\lambda)$ and $p_0^{(-)}(\lambda)$. Moreover, since, according to (3.4), the quantity Q_0 depends *linearly* on Γ , there exist three critical values of the parameter

$$\Gamma_0 = \frac{A^2B - AD - B\Delta - BG}{A - B},$$

$$\Gamma_{\pm} = \Gamma_0 \pm \frac{2\sqrt{\Delta(A^2B^2 + A^2D + B^2G)}}{A - B}$$

such that, when they are intersected, the type of these points changes. Namely,

- $\Gamma < \Gamma_-$: $\mathbf{x}_0^{(+)}$ — stable node, $\mathbf{x}_0^{(-)}$ — unstable node (Fig. 4a);
- $\Gamma_- < \Gamma < \Gamma_0$: $\mathbf{x}_0^{(+)}$ — stable focus, $\mathbf{x}_0^{(-)}$ — unstable focus (Fig. 4b);
- $\Gamma_0 < \Gamma < \Gamma_+$: $\mathbf{x}_0^{(+)}$ — unstable focus, $\mathbf{x}_0^{(-)}$ — stable focus (Figs. 4c–4f);
- $\Gamma_+ < \Gamma$: $\mathbf{x}_0^{(+)}$ — unstable node, $\mathbf{x}_0^{(-)}$ — stable node (Fig. 4g).

It can also be shown that, as Γ_0 is intersected, the Andronov–Hopf bifurcation occurs, resulting in a pair of limit cycles: a stable limit cycle in a neighborhood of $\mathbf{x}_0^{(+)}$ and an unstable one in a neighborhood of $\mathbf{x}_0^{(-)}$, see Fig. 4c. Next, as Γ increases, these cycles increase in size and, at some value of the parameter

$$\Gamma = \Gamma_* < \Gamma_+,$$

reach the fixed points $\mathbf{x}_{\pi}^{(+)}$ and $\mathbf{x}_{\pi}^{(-)}$ to form two pairs of separatrices to each of the points, Fig. 4d. As Γ increases further, two pairs of limit cycles appear on the torus, one pair being stable and the other pair unstable (all cycles are nonhomotopic to a point), see Fig. 4e. Then at some value of the parameter

$$\Gamma_* < \Gamma = \Gamma_{**} < \Gamma_+,$$

as a result of a tangent bifurcation, all 4 cycles disappear simultaneously, see Fig. 4f. Next, when $\Gamma = \Gamma_+$, the points $\mathbf{x}_0^{(+)}$ and $\mathbf{x}_0^{(-)}$ turn from foci into nodes, see Fig. 4g. We note that in Fig. 4 the separatrices to the points $\mathbf{x}_{\pi}^{(+)}$ and $\mathbf{x}_{\pi}^{(-)}$ divide the torus \mathbb{T}^2 into several invariant regions.

The same types of phase portraits arise under changes in Γ when

$$\Delta < 0,$$

but in this case $\mathbf{x}_0^{(+)}$ and $\mathbf{x}_0^{(-)}$ are saddles and the points $\mathbf{x}_{\pi}^{(+)}$ and $\mathbf{x}_{\pi}^{(-)}$ turn out to be foci or nodes, respectively. Generally speaking, numerical investigations show that the following hypothesis holds:

in the generic case (i. e., when the parameters do not satisfy the conditions of bifurcation), the reduced system (3.3) has one of the six generic types of phase portraits in Fig. 4 (i. e., the portrait 4d is excluded).

Remark 7. The problem with the proof of this statement is to prove that there exists the only tangent bifurcation of the appearance (disappearance) of two pairs of limit cycles in the system (2.14) for $k_1 = k_2 = 0$.

The motion of the Roller Racer in the fixed coordinate system OXY is defined by the system (2.16). Investigation of this system is a separate problem (which we do not consider in this paper). We only note that the existence of limit cycles in the reduced system leads to the situation where the inertial motion of the wheeled vehicle does not tend to rectilinear motion as $t \rightarrow \pm\infty$ (see Fig. 5), which is opposed to that of the Chaplygin sleigh (see, e.g., [35]).

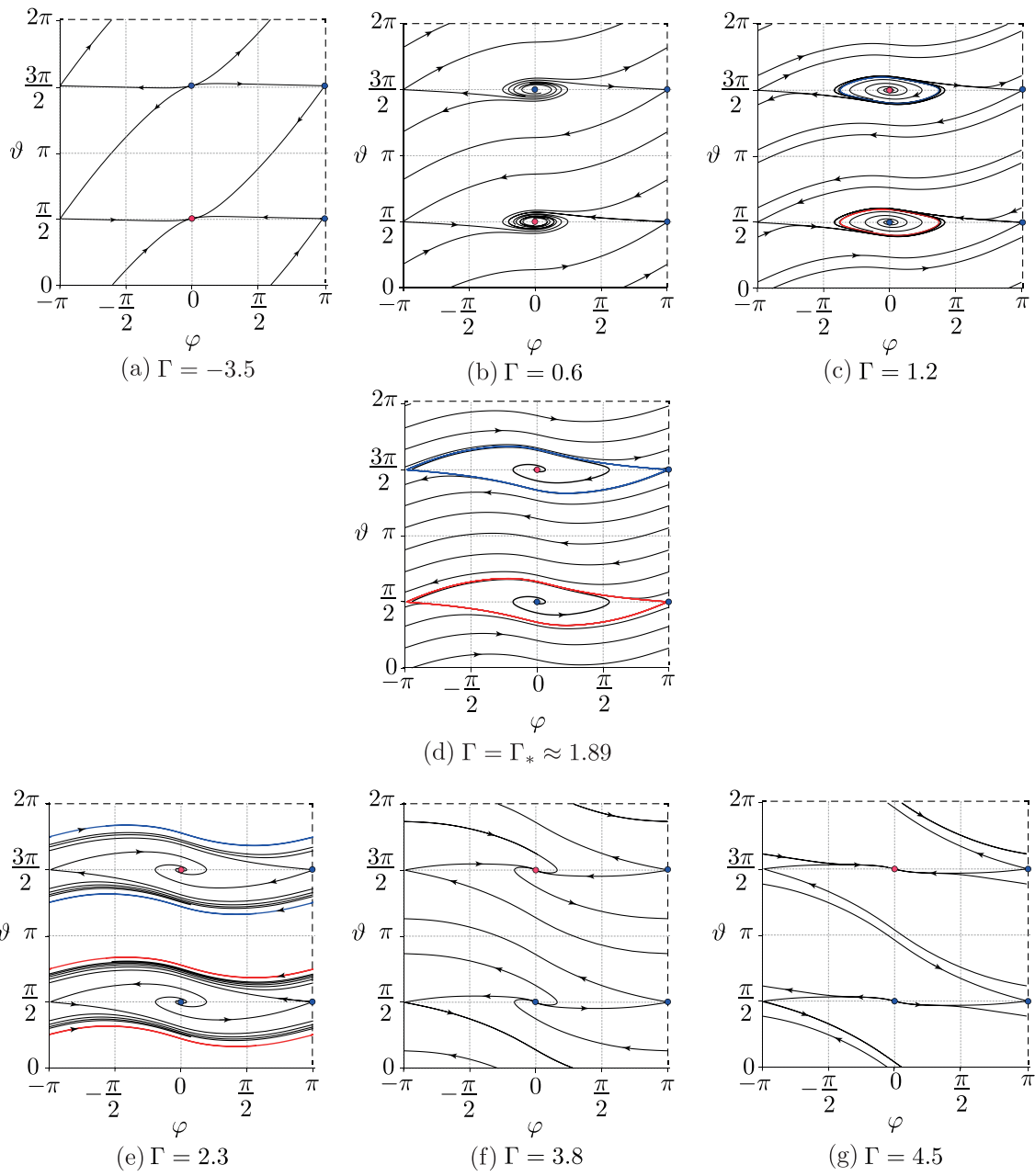


Fig. 4. Phase portrait of the system (3.3) for the fixed $A = 3$, $B = 1$, $D = 2$, $G = 1$, $h = 1$, $\Delta = 0.5$ and different values of Γ . Red and dark blue denote, respectively, stable and unstable limit cycles, and fixed points (in this case $\Gamma_0 = \frac{3}{4}$, $\Gamma_{\pm} = \frac{3}{4} \pm \sqrt{14}$).

4. CRITERION FOR ACCELERATION OF A ROLLER RACER WITH PERIODIC EXCITATION

In Section 3 it was shown (see Proposition 2) that, if $k_1 = k_2 = 0$, then the phase space \mathcal{M}_r^3 of the reduced system (2.14) is foliated by two-dimensional tori \mathbb{T}^2 on which there always exists an asymptotically stable fixed point. As a result, a degenerate one-parameter family of asymptotically stable fixed points Σ^1 arises in the space \mathcal{M}_r^3 . As above, we will assume that

$$\Delta > 0, \quad A^2B^2 + A^2D + B^2G > 0,$$

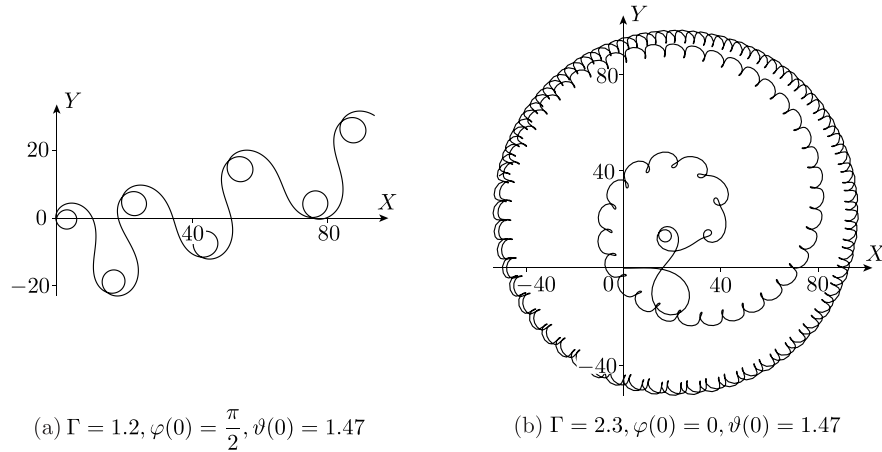


Fig. 5. A typical view of the trajectory of point P for the fixed parameters $A = 3, B = 1, D = 2, G = 1, h = 1, \Delta = 0.5, c_2 = 1$ in a neighborhood of stable limit cycles.

then this family is given as follows:

$$\Sigma^1 = \{(v, u, \varphi) \mid u = 0, \varphi = 0\} \subset \mathcal{M}_r^3,$$

where $v \in (0, +\infty)$ if $Q_0 > 0$ and $v \in (-\infty, 0)$ if $Q_0 < 0$. Recall that, according to (3.4):

$$Q_0 = A^2 B - AD - A\Gamma - B\Delta - BG + B\Gamma.$$

We now consider how the T -periodically time-dependent gyrostatic momenta

$$k_1(t+T) = k_1(t), \quad k_2(t+T) = k_2(t)$$

affects the trajectories of the system (2.14) with initial conditions from a small neighborhood of Σ^1 .

In this case, the energy (3.1) is not preserved, and therefore the phase space \mathcal{M}_r^3 is no longer foliated by two-dimensional submanifolds. However, from a physical point of view it is clear that, at sufficiently large values of velocities (energy) the contribution of the gyrostatic momenta turns out to be a small quantity. Consequently, the trajectories with initial conditions in a small neighborhood of Σ^1 with large values of the parameter v must remain in this neighborhood for a sufficiently long time. In the general case, the velocity v can both increase and decrease.

Our aim is:

to find conditions under which the absolute value of the velocity v will indefinitely increase for trajectories in a neighborhood of Σ^1 .

Poincaré transformation and reduction to the problem of stability. Let us define the angular coordinate $\psi = t \bmod T$ and rewrite the reduced system (2.14) in the form of the autonomous system

$$\begin{aligned} \frac{dv}{dt} &= uW + \sin \varphi f(\psi, \varphi), & \frac{du}{dt} &= -vW + g(\psi, \varphi), \\ \frac{d\varphi}{dt} &= \frac{\sqrt{J(\varphi)}}{\sqrt{\Phi(\varphi)}} u, & \frac{d\psi}{dt} &= 1, \end{aligned} \tag{4.1}$$

which is defined on $\mathbb{R}_{v,u}^2 \times \mathbb{T}^2$.

As can be seen, for the trajectories lying in Σ^1 the relation $Q_0 v > 0$ holds. Taking this into account, we make a change of variables and rescale time:

$$x = \frac{1}{Q_0 v}, \quad y = \frac{u}{Q_0 v}, \quad d\tau = Q_0 v dt. \tag{4.2}$$

In the new variables the system (4.1) has the form

$$\begin{aligned} \frac{dx}{d\tau} &= xy \left[\frac{yZ(\varphi)}{\Phi(\varphi)\sqrt{J(\varphi)}} - \frac{\Delta \sin \varphi}{Q_0 \sqrt{J(\varphi)\Phi(\varphi)}} \right] - x^3 \sin \varphi f(\psi, \varphi), \\ \frac{dy}{d\tau} &= (Q_0^{-2} + y^2) \left[\frac{yZ(\varphi)}{\Phi(\varphi)\sqrt{J(\varphi)}} - \frac{\Delta \sin \varphi}{Q_0 \sqrt{J(\varphi)\Phi(\varphi)}} \right] - x^3 \sin \varphi f(\psi, \varphi) + Q_0^{-1} g(\psi, \varphi) x^2, \\ \frac{d\varphi}{d\tau} &= \frac{\sqrt{J(\varphi)}}{Q_0 \sqrt{\Phi(\varphi)}} y, \quad \frac{d\psi}{d\tau} = \frac{x}{Q_0}. \end{aligned} \quad (4.3)$$

In this case, according to (4.2), the coordinates x and y belong to the half-plane $\mathbb{R}_+^2 = \{(x, y) \mid x \geq 0\}$ so that the phase space of the system (4.3) is a four-dimensional manifold with boundary

$$\mathcal{M}^4 = \mathbb{R}_+^2 \times \mathbb{T}^2 = \{(x, y, \varphi, \psi) \mid x \in [0, +\infty), y \in (-\infty, +\infty), \varphi \bmod 2\pi, \psi \bmod T\}.$$

Its boundary $x = 0$ is an invariant submanifold of the system (4.3). It corresponds to “the points at infinity” of the initial system (2.14) for which $Q_0 v \rightarrow +\infty$.

Remark 8. For polynomial systems on a plane the transformation of coordinates and time of the form (4.2) is usually called the Poincaré transformation [41].

Remark 9. As can be seen, on the submanifold $x = 0$ the equations of motion for the variables y and φ in the system (4.3) are identical to those in the case of absence of rotors ($f \equiv 0, g \equiv 0$). Hence, the results obtained in Section 3 on the existence of asymptotically stable fixed points and limit cycles remain valid for the submanifold $x = 0$. In order to pass to the system (3.3), the following transformation needs to be made:

$$y = (Q_0 \tan \vartheta)^{-1}, \quad dt = Q_0^2 \sqrt{2h} \sin \vartheta d\tau.$$

The system (4.3) has a one-parameter family of fixed points given by the relations

$$x = 0, \quad y = 0, \quad \varphi = 0, \quad (4.4)$$

i.e., it is parameterized by the variable ψ . In a neighborhood of these fixed points the system can be represented as

$$\begin{aligned} \frac{d\mathbf{r}}{d\tau} &= \mathbf{A}\mathbf{r} + \mathbf{F}(\mathbf{r}, \psi), \quad \frac{d\psi}{d\tau} = \frac{x}{Q_0}, \\ \mathbf{r} &= (x, y, \varphi), \quad \mathbf{A} = \begin{pmatrix} 0 & 0 & 0 \\ 0 & \frac{Z(0)}{Q_0^2 \Phi(0) \sqrt{J(0)}} & -\frac{\Delta}{Q_0^3 \sqrt{\Phi(0) J(0)}} \\ 0 & \frac{1}{Q_0} \sqrt{\frac{J(0)}{\Phi(0)}} & 0 \end{pmatrix}, \end{aligned} \quad (4.5)$$

where $\mathbf{F}(\mathbf{r}, \psi)$ is a periodic in ψ function whose expansion in terms of \mathbf{r} begins with terms of order 2 (see also [28]). It is important to keep in mind that we have chosen the transformation (4.2) in such a way that *both nonzero eigenvalues of the matrix \mathbf{A} have a negative real part*. (This is due to the fact that the family of stable fixed points of the unperturbed system Σ^1 after the transformation (4.2) satisfies the relations $x = 0$ and $\varphi = 0$.)

Thus, we have reduced the problem of the existence of accelerating trajectories to the problem of stability of the family (4.4) for the system with degenerate linear part (4.5).

In principle, this problem can be solved using the method presented in [4]. In this case, it is necessary to make several steps of the Poincaré–Dulac normalization for the vector equation of the system (4.5) and then to exclude, by a suitable transformation with an averaging procedure,

the dependence on ψ . But this approach is rather time-consuming, so in this paper we will obtain a criterion for speedup by analyzing the restriction of the system to the central manifold [28, 30] and will not give a rigorous proof.

Restriction of the system to the central manifold. It follows from the aforesaid that, for each fixed point of the family (4.4), the spectrum of the linear part of the system (4.5) contains a pair of zero eigenvalues and a pair of eigenvalues with negative real part. As a result, according to the central manifold theorem [14], there exists a two-dimensional invariant central manifold \mathcal{M}_c^2 such that in a neighborhood of (4.4)

$$\mathcal{M}_c^2 = \{(x, y, \varphi, \psi) \mid 0 < x < \varepsilon, \psi \bmod T, y = \eta(x, \psi) = O(x^N), \varphi = \xi(x, \psi) = O(x^N)\},$$

for some ε and $N \geq 2$, and the trajectories of the system (4.5) in a neighborhood of \mathcal{M}_c^2 approach it exponentially. We approximate \mathcal{M}_c^2 using a series in powers of x (see, e.g., [28])

$$y = \sum_{k=2}^3 \alpha_k(\psi)x^k + O(x^4), \quad \varphi = \sum_{k=2}^3 \beta_k(\psi)x^k + O(x^4). \quad (4.6)$$

Substituting this expansion into the corresponding equations of the system (4.3) and equating the coefficients with equal powers of x , we find:

$$\begin{aligned} \alpha_2 &= 0, \quad \alpha_3 = \Phi(0) \frac{Q_0^2}{\Delta} \frac{dg_0}{d\psi}, \quad g_0 = g(0, \psi), \\ \beta_2 &= \sqrt{J(0)\Phi(0)} \frac{Q_0^2 g_0}{\Delta}, \quad \beta_3 = Z(0) \sqrt{\Phi(0)} \frac{Q_0^3}{\Delta^2} \frac{dg_0}{d\psi}. \end{aligned} \quad (4.7)$$

Next, using (4.6) we obtain a restriction of the system (4.3) in the following form:

$$\begin{aligned} \frac{dx}{d\tau} &= \gamma(\psi)x^5 + O(x^6), \quad \frac{d\psi}{d\tau} = \frac{x}{Q_0}, \\ \gamma &= f(0, \psi)\beta_2 = \frac{Q_0^2}{\Delta(A-B)^3} \left[\frac{dk_2}{d\psi} + \frac{dk_2}{d\psi} \right] \left[A \frac{dk_2}{d\psi} + B \frac{dk_2}{d\psi} \right]. \end{aligned} \quad (4.8)$$

Remark 10. The expansion in the form (4.6) can be continued up to higher order in x . The coefficients of this expansion are calculated at each step from the system of algebraic (nondifferential) equations.

Nonlinear speedup at large velocities. Let $x \ll 1$, then, neglecting in the first equation of (4.3) the terms of order $O(x^6)$, we divide it by the second equation. Next, after averaging over ψ and passing to the initial time t , we obtain

$$\begin{aligned} \frac{dx}{dt} &= Q_0 \langle \gamma \rangle x^4, \quad \langle \gamma \rangle = \frac{1}{T} \int_0^T \gamma(t) dt, \\ \gamma(t) &= \frac{Q_0^2}{\Delta(A-B)^3} (A \dot{k}_2^2 + B \dot{k}_1^2 + (A+B) \dot{k}_1 \dot{k}_2). \end{aligned}$$

If $Q_0 \langle \gamma \rangle < 0$, then, using (4.7) we find the following asymptotics:

$$\begin{aligned} x(t) &= \frac{t^{-1/3}}{(-3Q_0 \langle \gamma \rangle)^{1/3}} + o(t^{-1/3}), \quad \varphi(t) = -\frac{Q_0^2 (A \dot{k}_2 + B \dot{k}_1)}{\Delta(A-B)(-3Q_0 \langle \gamma \rangle)^{2/3}} t^{-2/3} + o(t^{-2/3}), \\ y(t) &= -\frac{Q_0 \sqrt{A^2 B^2 + A^2 D + B^2 G}}{\Delta(A-B)^2 \langle \gamma \rangle} (A \ddot{k}_2 + B \ddot{k}_1) t^{-1} + o(t^{-1}). \end{aligned}$$

Returning to the initial variables v and u , we obtain the following result.

Acceleration criterion. Let

$$c = -\frac{3Q_0^3}{\Delta(A-B)^3 T} \int_0^T (A\dot{k}_2^2 + B\dot{k}_1^2 + (A+B)\dot{k}_1\dot{k}_2) dt > 0, \quad (4.9)$$

then there exists a sufficiently small $\varepsilon > 0$, and u_0 and φ_0 are constant, so that, for the trajectories of the system (2.14) with the initial conditions $\frac{1}{\varepsilon} < vQ_0$, $|u| < u_0\varepsilon^2$, $|\varphi| < \varphi_0\varepsilon^2$, we have $v(t) \rightarrow +\infty$, $u(t) \rightarrow 0$, $\varphi(t) \rightarrow 0$ as $t \rightarrow +\infty$:

$$\begin{aligned} v(t) &= \frac{(ct)^{1/3}}{Q_0} + o(t^{1/3}), \quad \varphi(t) = -\frac{Q_0^2 \dot{\kappa}(t)}{\Delta(A-B)} (ct)^{-2/3} + o(t^{-2/3}), \\ u(t) &= -\frac{Q_0^2 (A^2 B^2 + A^2 D + B^2 G)^{1/2} \ddot{\kappa}(t)}{\Delta(A-B)^3} (ct)^{-2/3} + o(t^{-2/3}), \quad \kappa(t) = Ak_2(t) + Bk_1(t). \end{aligned} \quad (4.10)$$

If the rotor with varying momentum is carried only by one of the platforms (i.e., $\dot{k}_1\dot{k}_2 = 0$), then relation (4.9) reduces to the condition $Q_0 < 0$, i.e., the existence of speeding-up trajectories does not depend explicitly on the gyrostatic momentum, but is defined only by the parameters of the wheeled vehicle. Numerical experiments show that the found relations (4.10) describe well the behavior of trajectories with initial conditions that lie not only in the neighborhood of the manifold Σ^1 (see Fig. 6).

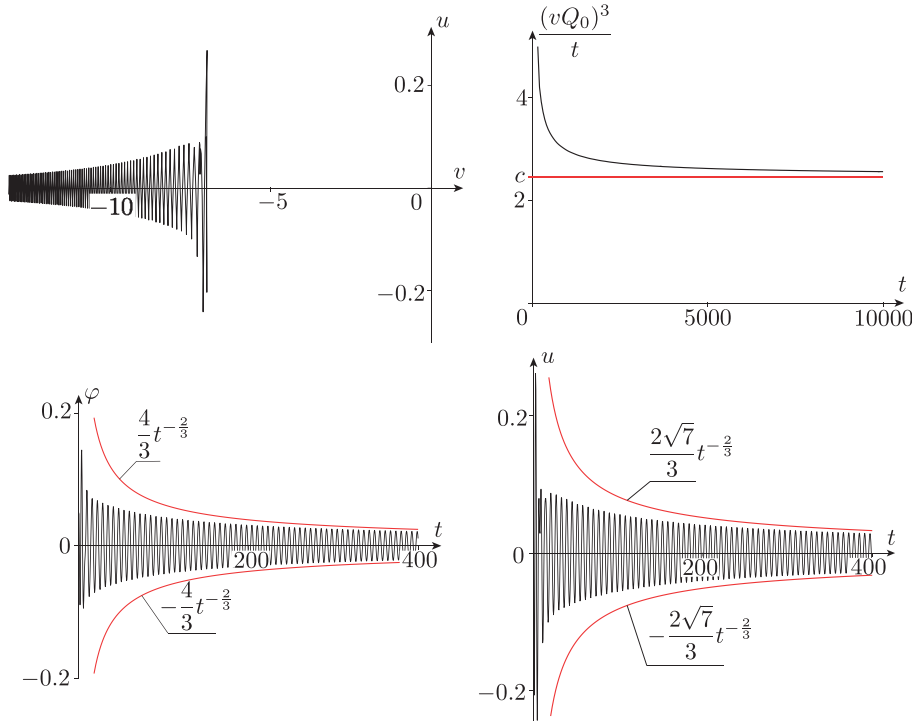


Fig. 6. Trajectories of the reduced system (2.14) for the fixed parameters $A = 3$, $B = 1$, $D = 2$, $G = 1$, $\Delta = 0.5$, $\Gamma = 1.2$ and $k_1 = 3 \sin t$, $k_2 = 0$ under the initial conditions $v(0) = -7$, $u(0) = 0.1$, $\varphi(0) = 0.05$. The red curves are the curves described by relations (4.10).

A typical trajectory of the point of attachment of the platforms P for which the velocity v increases indefinitely with time is shown in Fig. 7. As can be seen, in this case the wheeled vehicle moves “on average” along some straight line, while performing oscillations with a constant amplitude. Earlier, such speeding-up trajectories were encountered in the Chaplygin sleigh with varying mass distribution [6, 7].

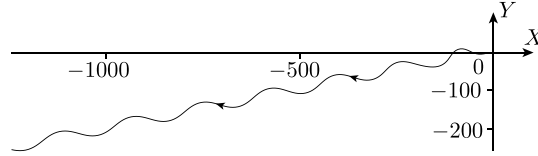


Fig. 7. Trajectory of point P in the fixed coordinate system for the initial conditions and parameters corresponding to Fig. 6 and $X(0) = 0$, $Y(0) = 0$, $\psi(0) = 0$, $c_2 = 1$.

We note that condition (4.9) must be satisfied for speeding-up trajectories arising only in a neighborhood of Σ^1 — stable equilibrium points of the reduced system without gyrostatic momentum. Apparently, trajectories speeding up without bound can also arise in a neighborhood of the limit cycles found in Section 3. Analysis of this is a separate problem.

Remark 11. Part of the circle on $\mathbb{R}_{v,u}^2$ corresponding to the fixed level of energy $E(u,v) = h(A - B)^2$ for which $Q_0 v > 0$ turns, after the transformation (4.2), into a hyperbola:

$$hx^2 - y^2 = 1.$$

Since the energy increases when condition (4.9) is satisfied, it can obviously be shown that all trajectories inside the asymptotes of this hyperbola tend to the point $x = y = 0$. That is to say, at some (sufficiently large) value of h the basin of attraction is given by the inequality

$$0 < hx^2 - y^2 \leq 1, \quad 0 < x.$$

5. NUMERICAL INVESTIGATIONS OF THE POINCARÉ MAP

In the preceding section it is shown that the problem of nonholonomic speedup of the Roller Racer can be solved explicitly. However, this solution provides no insight into the behavior of the trajectories of the system in general. Therefore, in this section we present the results of a short numerical analysis of the Poincaré map (more exactly, a stroboscopic map) of the reduced system (2.14).

Let us choose one of the simplest periodic perturbations of the system under which the rotor is located only on one of the platforms:

$$k_1(t) = k_0 \sin t, \quad k_2(t) = 0, \quad k_0 \geq 0. \quad (5.1)$$

In this case, the reduced system (2.14) depends 2π -periodically on time t and hence gives rise to a (global) three-dimensional Poincaré map:

$$\mathcal{P}^3 : \mathcal{M}_r^3 \rightarrow \mathcal{M}_r^3.$$

It follows from relations (2.15) that the functions $f(t, \varphi)$ and $g(t, \varphi)$ are symmetric with respect to the time reversal $t \rightarrow -t$ under the choice of a perturbation in the form (5.1). Therefore, the map \mathcal{P}^3 admits the involution

$$\sigma : u \rightarrow -u, \quad v \rightarrow -v.$$

This implies that, if \mathcal{M}_i is an invariant set of the map \mathcal{P}^3 , then either $\sigma(\mathcal{M}_i) = \mathcal{M}_i$ or there exists an additional invariant set $\widetilde{\mathcal{M}}_i = \sigma(\mathcal{M}_i)$. If the initial set \mathcal{M}_i of the map \mathcal{P}^3 was an attractor, then $\widetilde{\mathcal{M}}_i$ is a repeller, and vice versa.

The set of fixed points of involution σ forms a circle:

$$\text{Fix}\sigma = \{v = 0, u = 0, \varphi \bmod 2\pi\} \subset \mathcal{P}^3.$$

Remark 12. Involution σ generalizes involution $R^{(1)}$ from Section 3, but, as can be seen from Eqs. (2.14), the map \mathcal{P}^3 admits no generalization of involution $R^{(2)}$.

In performing the numerical analysis of the map \mathcal{P}^3 , we fix part of the parameters as follows:

$$A = 3, \quad B = 1, \quad D = 1, \quad G = \frac{1}{2}, \quad \Delta = 3, \quad (5.2)$$

and will change only the parameters k_0 and Γ .

Using relations (5.1) and (5.2) we find that the condition for the existence of unbounded trajectories described by the criterion from Section 4 can be represented as

$$c = -\frac{3Q_0^3 B k_0^2}{2\Delta(A-B)^3} = \frac{k_0^2}{2} (\Gamma - \Gamma_0)^3 > 0, \quad \Gamma_0 = 5/4.$$

Here Γ_0 coincides with the value of Γ at which the stability of point $\mathbf{x}_0^{(+)}$ from Section 3 is lost. Below we consider successively the situations $\Gamma < \Gamma_0$ and $\Gamma > \Gamma_0$.

Remark 13. It follows from inequalities (2.17) that physically admissible values of the parameter Γ , with (5.2) taken into account, lie in the interval $\Gamma \in \left(3 - \frac{30}{\sqrt{95}}, 3 + \frac{30}{\sqrt{95}}\right)$. Therefore, the values $\Gamma_{\pm} = 5/4 \pm \frac{\sqrt{222}}{2}$ at which the type of $\mathbf{x}_0^{(\pm)}$ changes lies outside the physical parameter space.

1. $\Gamma < \Gamma_0 = 5/4$. In this case, the criterion of nonlinear acceleration near Σ^1 is violated. Moreover, it turns out (this is observed in all numerical experiments) that for all trajectories of the system (2.14) the values of the variables u and v remain bounded as $t \rightarrow +\infty$. Obviously, by analogy with the acceleration criterion one can obtain an explicit criterion of boundedness of the velocities (energy) of the Roller Racer.

Figure 8 shows a chart of the largest Lyapunov exponent Λ_1 and a chart of dynamical regimes of the map \mathcal{P}^3 on the parameter plane (Γ, k_0) for the trajectory with initial conditions corresponding to motion from the state of rest:

$$v(0) = 0, \quad u(0) = 0, \quad \varphi(0) = 0.$$

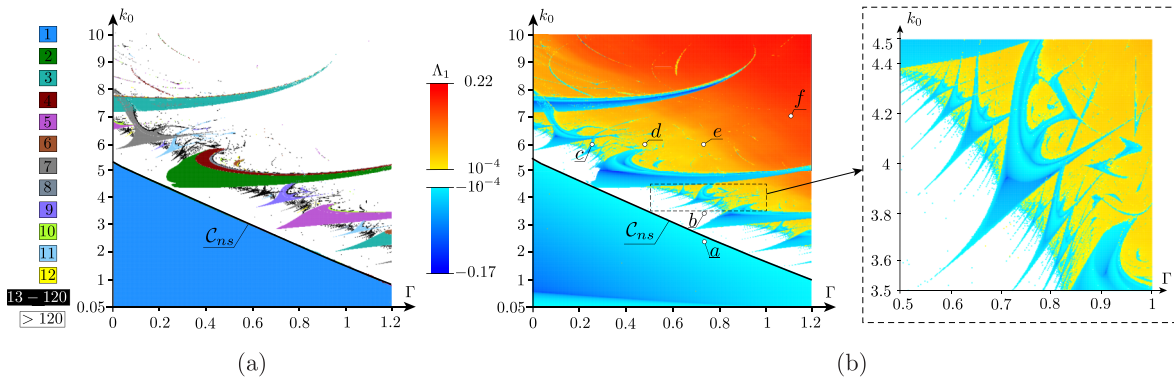


Fig. 8. Chart of dynamical regimes (a) in which different colors denote the periods of asymptotically stable fixed points of the map \mathcal{P}^3 (see the left panel with numbers of periods) and a chart of the largest Lyapunov exponent for the map \mathcal{P}^3 (b). Both charts are plotted on the parameter plane (Γ, k_0) and for fixed values of the other parameters (5.2); the right panel presents an enlarged fragment shown as a dashed line in the chart of the Lyapunov exponent.

Using these charts, we give a short description of the behavior of the trajectories of the system (2.14) depending on the parameters (Γ, k_0) , which is based on numerical analysis of the dynamics of the map \mathcal{P}^3 .

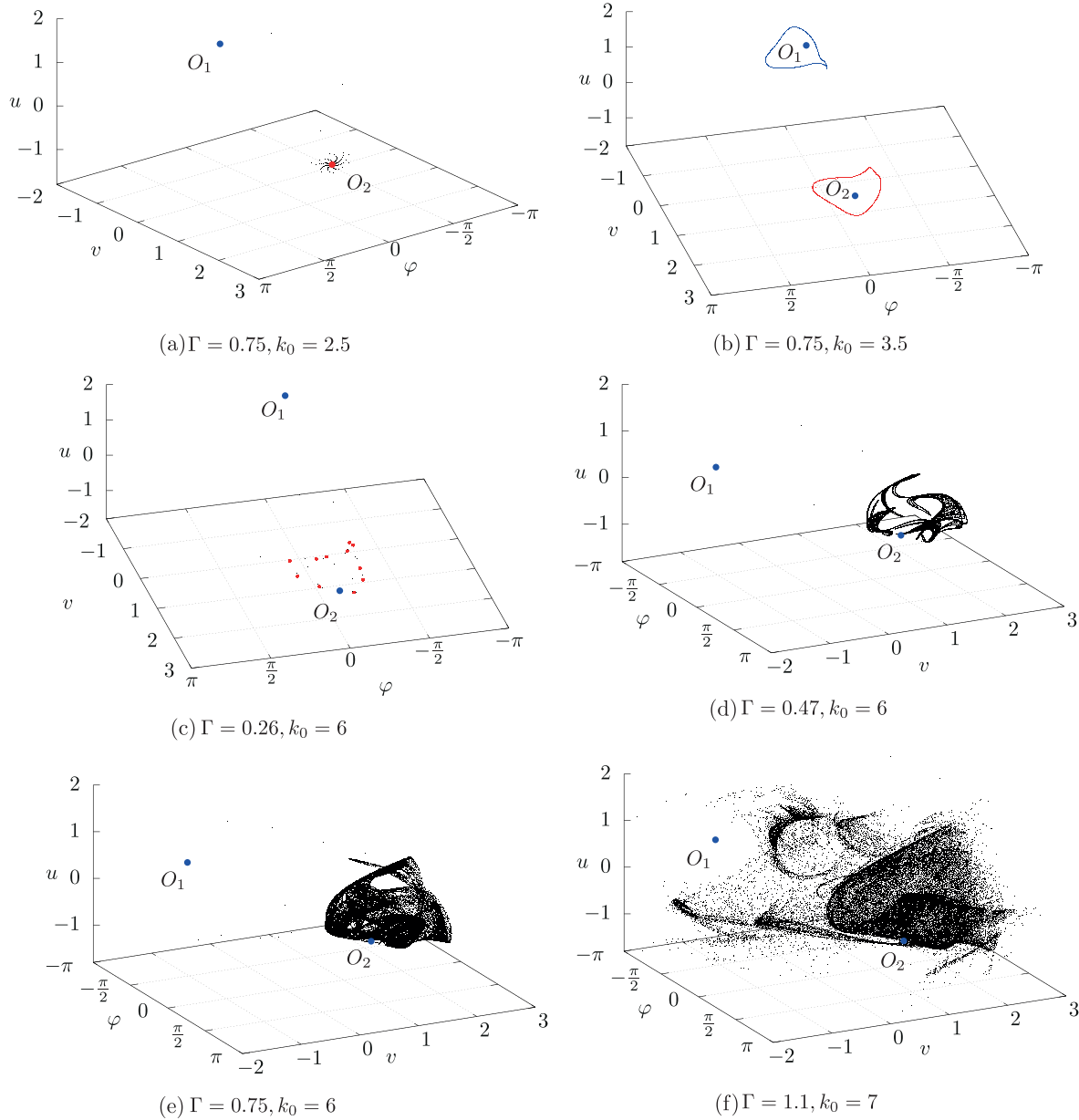


Fig. 9. Phase portraits of the Poincaré map \mathcal{P}^3 for the fixed parameter values (5.2) and different values of Γ and k_0 , which are shown as points (a)–(f) in Fig. 8b. Red and blue denote stable and unstable regular attractors, respectively.

- 1) On the plane of the parameters Γ and k_0 the bifurcation curve \mathcal{C}_{ns} is such that, if the point (Γ, k_0) lies under this curve, then the map \mathcal{P}^3 has only 2 fixed points, O_1 and O_2 , which are focus-nodes and are related by

$$\sigma(O_1) = O_2.$$

One of them is a global attractor, and the other is a global repeller (Fig. 9a). These points correspond to periodic solutions of the initial system (2.14).

- 2) As the parameter k_0 increases and the curve \mathcal{C}_{ns} is reached, the Neimark–Sacker bifurcation [42] of the above-mentioned periodic solutions occurs. Next, an asymptotically unstable invariant curve and an asymptotically stable invariant curve appear in a neighborhood of points O_1 and O_2 , respectively, on the map \mathcal{P}^3 (see Fig. 9b), which also turn out to be

a global attractor and a global repeller. Each of them corresponds to a torus in the initial system (2.14). These values of the parameters Γ and k_0 correspond to a fairly thin strip above the curve C_{ns} in Fig. 8; in this region white corresponds to tori with quasi-periodic trajectories. As is well known [44], this region is not homogeneous and is filled with “Arnold tongues”; inside them are the parameter values for which the invariant tori of the system (2.14) contain limit cycles with all possible rational rotation numbers.

- 3) It can be seen in Fig. 8b that, as k_0 decreases further, the “Arnold tongues” merge to form a (light blue) boundary of the white zone. When it is intersected, limit cycles arise on the invariant tori of the system (2.14), and the invariant curves of the map \mathcal{P}^3 break down into fixed points. Next, as we move into region $\Lambda_1 > 0$, the invariant tori lose smoothness and collapse [22].
- 4) Next, in a neighborhood of the stable invariant curve, by means of one of the scenarios described in [22], a strange attractor of torus-chaos type can arise (see, e.g., [22]), and in a neighborhood of the unstable cycle a repeller arises (see Figs. 9d and 10a). As can be seen from Fig. 8b, in the neighborhood of point d there are regions with a negative largest Lyapunov exponent Λ_1 which correspond to asymptotically stable fixed points. Thus, the attractor under consideration belongs to the so-called quasi-attractors [26]. The Lyapunov exponents for the trajectory in Fig. 9d are

$$\Lambda_1 \approx 0.036, \quad \Lambda_2 \approx -0.061, \quad \Lambda_3 \approx -0.484.$$

As can be seen, in this case $\Lambda_1 + \Lambda_2 < 0$ (this inequality was proposed in [23] as a nonrigorous criterion for an attractor to belong to quasi-attractors).

- 5) As the parameters Γ and k_0 increase further, a region (see Fig. 8b) arises in which no islands arise with negative Λ_1 and $\Lambda_1 + \Lambda_2 > 0$. The map \mathcal{P}^3 for this case is shown in Figs. 9e and 9f. The Lyapunov exponents for them are, respectively,

$$\Lambda_1 \approx 0.059, \quad \Lambda_2 \approx -0.035, \quad \Lambda_3 \approx -0.483$$

$$\Lambda_1 \approx 0.164, \quad \Lambda_2 \approx -0.043, \quad \Lambda_3 \approx -0.489.$$

Thus, in this case the attractor can belong to pseudo-hyperbolic attractors, but in order to show this, we need to use numerical criteria for verification of pseudo-hyperbolicity [23, 38]. At the same time, when the parameters increase considerably, the strange attractor can occupy such a large region in \mathcal{M}_r^3 (see Fig. 9f and Fig. 10b) that an intersection of the closures of the attractor and the repeller can arise, resulting in mixed dynamics [16, 21, 27], which apparently excludes pseudo-hyperbolic dynamics.

This description of possible dynamical regimes of the Roller Racer with periodic excitation is far from being complete: for certain parameters we have observed doubling of the invariant tori of the system (2.14). Generally speaking, a more detailed investigation of the scenarios of transition to chaotic dynamics (including mixed dynamics) in the system considered is a separate problem.

The problem of reconstructing the motion of the Roller Racer along the trajectories of the reduced system also requires a separate analysis, see [11]. Here we only illustrate the difference of the trajectory of the point of articulation of the platforms P for regular (a) and chaotic (b) trajectories of the reduced system, Fig. 11.

2. $\Gamma > \Gamma_0 = 5/4$. Numerical experiments show that the above-mentioned regular and chaotic regimes of motion persist in this case also. Therefore, we restrict ourselves here to showing that there exist parameter values at which in the phase space of the map \mathcal{P}^3 there coexist unbounded trajectories (i.e., those corresponding to the speedup of the Roller Racer) and chaotic trajectories of the reduced system, see Figs. 12 and 13.

The initial conditions for which a trajectory is unbounded are shown in gray in Figs. 12 and 13. As can be seen from Fig. 12, an unstable invariant curve lies on the boundary between the bounded and unbounded trajectories (they are shown in dark blue).

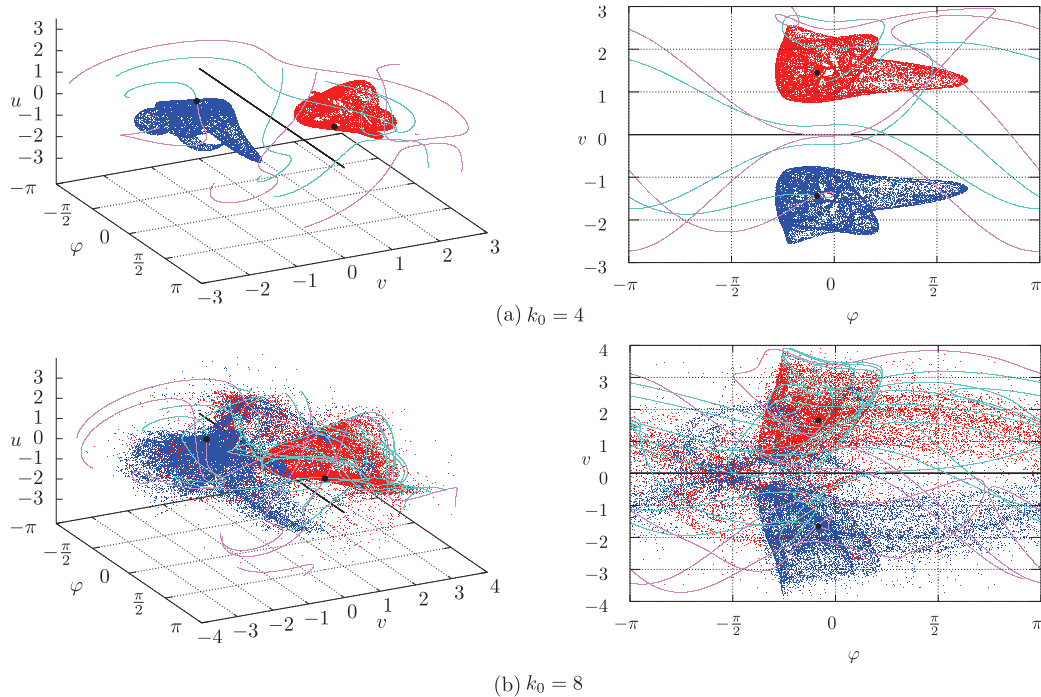


Fig. 10. Two phase portraits of the Poincaré map \mathcal{P}^3 for the fixed parameter values (5.2) and $\Gamma = 1.14$ and different values of k_0 , which demonstrate an expansion of the regions occupied by a strange attractor and a repeller, and the possibility of their “intersection”. Red and blue denote iterations of the map, respectively, in forward and backward time. Black denotes the fixed points O_1 and O_2 , turquoise and pink denote the one-dimensional separatrices of point O_1 , the black line indicates $\text{Fix}\sigma$, the line of the fixed points of involution σ .

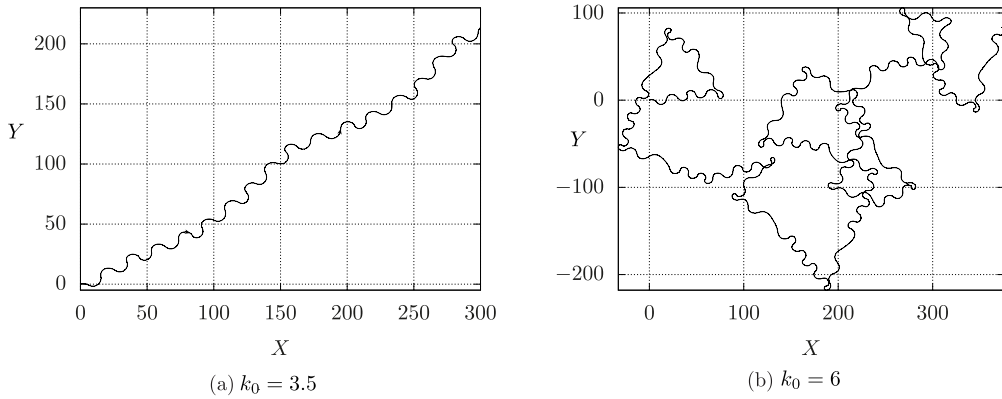


Fig. 11. The trajectory of point P in the fixed coordinate system for the parameter values (5.2) and $\Gamma = 0.75$.

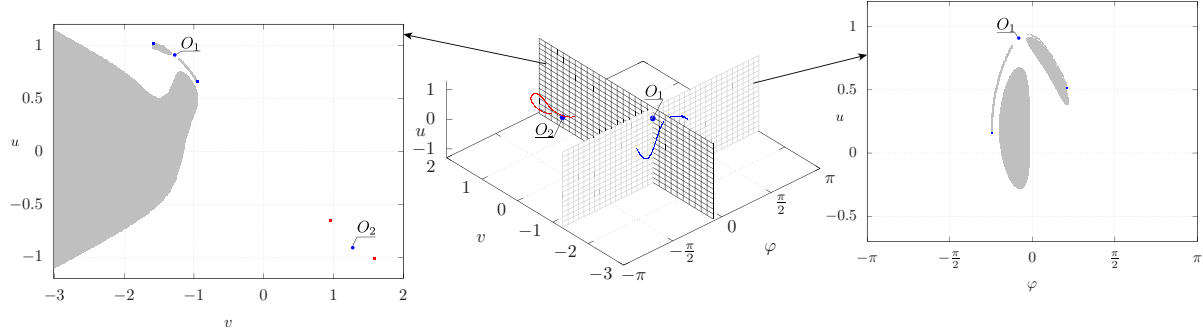


Fig. 12. The central panel shows a phase portrait of the Poincaré map \mathcal{P}^3 for the fixed parameter values (5.2) and $\Gamma = 1.4$, $k_0 = 0.97$, the right and left panels show thin layers (several pixels) of this portrait in a neighborhood of the corresponding planes. Gray denotes initial conditions for unbounded trajectories. The portrait shows invariant curves, one of which is an attractor (red), and the other is a repeller (dark blue).

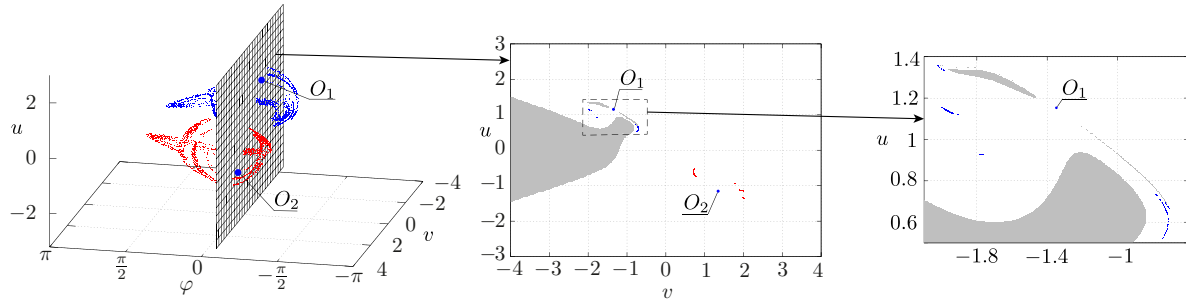


Fig. 13. The left panel shows a phase portrait of the Poincaré map \mathcal{P}^3 for the fixed parameter values (5.2) and $\Gamma = 1.4$, $k_0 = 2.4$, the central panel shows a thin layer of this portrait (several pixels) in a neighborhood of the corresponding plane, and the right panel enlarges the fragment depicted in the central panel. Gray denotes initial conditions for unbounded trajectories. The portrait also shows a strange attractor (red) and a strange repeller (dark blue).

Remark 14. If $\dot{k}_1 = \text{const}$, $\dot{k}_2 = \text{const}$, i.e., the gyrostatic momentum increases linearly with time t , then the system (2.14) reduces to analysis of a three-dimensional vector field. It can be shown that in this case the equations of motion possess equilibrium points which, in contrast to the fixed points of the map \mathcal{P}^3 , are defined by explicit relations.

ACKNOWLEDGMENTS

The authors extend their gratitude to Sergey V. Gonchenko and Alexey O. Kazakov for fruitful discussions.

FUNDING

The work of I. A. Bizyaev (Sections 3 and 4) was supported by the Russian Science Foundation (No. 21-71-10039). The work of I. S. Mamaev (Sections 2 and 5) was carried out within the framework of the state assignment of the Ministry of Science and Higher Education of Russia (FZZN-2020-0011).

CONFLICT OF INTEREST

The authors declare that they have no conflicts of interest.

REFERENCES

1. Ariel, G. and Schiff, J., Conservative, Dissipative and Super-Diffusive Behavior of a Particle Propelled in a Regular Flow, *Phys. D*, 2020, vol. 411, 132584, 9 pp.
2. Artemova, E. M., Karavaev, Yu. L., Mamaev, I. S., and Vetchanin, E. V., Dynamics of a Spherical Robot with Variable Moments of Inertia and a Displaced Center of Mass, *Regul. Chaotic Dyn.*, 2020, vol. 25, no. 6, pp. 689–706.
3. Bizyaev, I. A., The Inertial Motion of a Roller Racer, *Regul. Chaotic Dyn.*, 2017, vol. 22, no. 3, pp. 239–247.
4. Bizyaev, I., Bolotin, S., and Mamaev, I., Normal Forms and Averaging in an Acceleration Problem in Nonholonomic Mechanics, *Chaos*, 2021, vol. 31, no. 1, 013132, 16 pp.
5. Bizyaev, I. A., Borisov, A. V., and Mamaev, I. S., Exotic Dynamics of Nonholonomic Roller Racer with Periodic Control, *Regul. Chaotic Dyn.*, 2018, vol. 23, nos. 7–8, pp. 983–994.
6. Bizyaev, I. A., Borisov, A. V., and Mamaev, I. S., The Chaplygin Sleigh with Parametric Excitation: Chaotic Dynamics and Nonholonomic Acceleration, *Regul. Chaotic Dyn.*, 2017, vol. 22, no. 8, pp. 955–975.
7. Bizyaev, I. A., Borisov, A. V., Kozlov, V. V., and Mamaev, I. S., Fermi-Like Acceleration and Power-Law Energy Growth in Nonholonomic Systems, *Nonlinearity*, 2019, vol. 32, no. 9, pp. 3209–3233.

8. Bizyaev, I. A., Borisov, A. V., and Kuznetsov, S. P., The Chaplygin sleigh with friction moving due to periodic oscillations of an internal mass, *Nonlinear Dyn.*, 2019, vol. 95, no. 1, pp. 699–714.
9. Borisov, A. V., Kilin, A. A., and Mamaev, I. S., Invariant Submanifolds of Genus 5 and a Cantor Staircase in the Nonholonomic Model of a Snakeboard, *Internat. J. Bifur. Chaos Appl. Sci. Engrg.*, 2019, vol. 29, no. 3, 1930008, 19 pp.
10. Borisov, A. V., Kilin, A. A., and Mamaev, I. S., On the Hadamard–Hamel Problem and the Dynamics of Wheeled Vehicles, *Regul. Chaotic Dyn.*, 2015, vol. 20, no. 6, pp. 752–766.
11. Borisov, A. V., Kilin, A. A., and Mamaev, I. S., The Problem of Drift and Recurrence for the Rolling Chaplygin Ball, *Regul. Chaotic Dyn.*, 2013, vol. 18, no. 6, pp. 832–859.
12. Borisov, A. V. and Mamaev, I. S., Symmetries and Reduction in Nonholonomic Mechanics, *Regul. Chaotic Dyn.*, 2015, vol. 20, no. 5, pp. 553–604.
13. Bravo-Doddoli, A. and García-Naranjo, L. C., The Dynamics of an Articulated n -Trailer Vehicle, *Regul. Chaotic Dyn.*, 2015, vol. 20, no. 5, pp. 497–517.
14. Carr, J., *Applications of Centre Manifold Theory*, Appl. Math. Sci., vol. 35, New York: Springer, 1981.
15. Chakon, O. and Or, Y., Analysis of Underactuated Dynamic Locomotion Systems Using Perturbation Expansion: The Twistcar Toy Example, *J. Nonlinear Sci.*, 2017, vol. 27, no. 4, pp. 1215–1234.
16. Chigarev, V., Kazakov, A., and Pikovsky, A., Kantorovich–Rubinstein–Wasserstein Distance between Overlapping Attractor and Repeller, *Chaos*, 2020, vol. 30, no. 7, 073114, 10 pp.
17. Emelianova, A. A. and Nekorkin, V. I., The Third Type of Chaos in a System of Two Adaptively Coupled Phase Oscillators, *Chaos*, 2020, vol. 30, no. 5, 051105, 8 pp.
18. Gelfreich, V. and Turaev, D., Unbounded Energy Growth in Hamiltonian Systems with a Slowly Varying Parameter, *Comm. Math. Phys.*, 2008, vol. 283, no. 3, pp. 769–794.
19. Gonchenko, S. V., Dynamical Systems with Homoclinic Tangencies, Ω -Moduli and Bifurcations, *Doctoral Dissertation*, Nizhni Novgorod, National Research Lobachevsky State University of Nizhni Novgorod, 2004, 300 pp. (Russian).
20. Gonchenko, A. S., Gonchenko, S. V., and Kazakov, A. O., Richness of Chaotic Dynamics in the Nonholonomic Model of Celtic Stone, *Regul. Chaotic Dyn.*, 2013, vol. 18, no. 5, pp. 521–538.
21. Gonchenko, A. S., Gonchenko, S. V., Kazakov, A. O., and Turaev, D. V., On the Phenomenon of Mixed Dynamics in Pikovsky–Topaj System of Coupled Rotators, *Phys. D*, 2017, vol. 350, pp. 45–57.
22. Gonchenko, A. S., Gonchenko, S. V., and Shilnikov, L. P., Towards Scenarios of Chaos Appearance in Three-Dimensional Maps, *Nelin. Dinam.*, 2012, vol. 8, no. 1, pp. 3–28 (Russian).
23. Gonchenko, S. V., Kazakov, A. O., Turaev, D. V., and Kaynov, M. N., On Methods for Verification of the Pseudohyperbolicity of Strange Attractors, *Izv. Vyssh. Uchebn. Zaved. Prikl. Nelin. Dinam.*, 2021, vol. 29, no. 1, pp. 160–185 (Russian).
24. Gonchenko, S. V. and Ovsyannikov, I. I., On Bifurcations of Three-Dimensional Diffeomorphisms with a Non-Transversal Heteroclinic Cycle Containing Saddle-Foci, *Nelin. Dinam.*, 2010, vol. 6, no. 1, pp. 61–77 (Russian).
25. Gonchenko, S. V., Ovsyannikov, I. I., Simó, C., and Turaev, D., Three-Dimensional Hénon-Like Maps and Wild Lorenz-Like Attractors, *Internat. J. Bifur. Chaos Appl. Sci. Engrg.*, 2005, vol. 15, no. 11, pp. 3493–3508.
26. Gonchenko, S. V., Shil'nikov, L. P., and Turaev, D. V., Quasiattractors and Homoclinic Tangencies. Computational Tools of Complex Systems: 1, *Comput. Math. Appl.*, 1997, vol. 34, nos. 2–4, pp. 195–227.
27. Gonchenko, S. V. and Turaev, D. V., On Three Types of Dynamics and the Notion of Attractor, *Proc. Steklov Inst. Math.*, 2017, vol. 297, no. 1, pp. 116–137; see also: *Tr. Mat. Inst. Steklova*, 2017, vol. 297, pp. 133–157.
28. Guckenheimer, J. and Holmes, P., *Nonlinear Oscillations, Dynamical Systems, and Bifurcations of Vector Fields*, Appl. Math. Sci., vol. 42, New York: Springer, 1983.
29. Halvani, O. and Or, Y., Nonholonomic Dynamics of the Twistcar Vehicle: Asymptotic Analysis and Hybrid Dynamics of Frictional Skidding, *Nonlinear Dyn.*, 2022, vol. 107, no. 4, pp. 3443–3459.
30. Hirsch, M. W., Pugh, C. C., and Shub, M., *Invariant Manifolds*, Lecture Notes in Math., vol. 583, New York: Springer, 1977.
31. Ito, S., Sugiura, S., Masuda, Y., Nohara, S., and Morita, R., Mechanism and Control of a One-Actuator Mobile Robot Incorporating a Torque Limiter, *J. Intell. Robot. Syst.*, 2020, vol. 97, no. 2, pp. 431–448.
32. Kazakov, A., Merger of a Hénon-Like Attractor with a Hénon-Like Repeller in a Model of Vortex Dynamics, *Chaos*, 2020, vol. 30, no. 1, 011105, 7 pp.

33. Kazakov, A. O., Strange Attractors and Mixed Dynamics in the Unbalanced Rubber Ball on a Plane Problem, *Regul. Chaotic Dyn.*, 2013, vol. 18, no. 5, pp. 508–520.
34. Kilin, A. A. and Pivovarova, E. N., Chaplygin Top with a Periodic Gyrostatic Moment, *Rus. J. Math. Phys.*, 2018, vol. 25, no. 4, pp. 509–524.
35. Kozlov, V. V., The Phenomenon of Reversal in the Euler–Poincaré–Suslov Nonholonomic Systems, *J. Dyn. Control Syst.*, 2016, vol. 22, no. 4, pp. 713–724.
36. Krishnaprasad, P. S. and Tsakiris, D. P., Oscillations, SE(2)-Snakes and Motion Control: A Study of the Roller Racer, *Dyn. Syst.*, 2001, vol. 16, no. 4, pp. 347–397.
37. Kuleshov, A. S., Further Development of the Mathematical Model of a Snakeboard, *Regul. Chaotic Dyn.*, 2007, vol. 12, no. 3, pp. 321–334.
38. Kuznetsov, S. P. and Kruglov, V. P., Verification of Hyperbolicity for Attractors of Some Mechanical Systems with Chaotic Dynamics, *Regul. Chaotic Dyn.*, 2016, vol. 21, no. 2, pp. 160–174.
39. Mamaev, I. S. and Vetchanin, E. V., Dynamics of Rubber Chaplygin Sphere under Periodic Control, *Regul. Chaotic Dyn.*, 2020, vol. 25, no. 2, pp. 215–236.
40. Ostrowski, J., Lewis, A., Murray, R., and Burdick, J., Nonholonomic Mechanics and Locomotion: The Snakeboard Example, in *Proc. of the IEEE Internat. Conf. on Robotics and Automation (San Diego, Calif., May 1994)*, pp. 2391–2397.
41. Perko, L., *Differential Equations and Dynamical Systems*, 3rd ed., Texts Appl. Math., vol. 7, New York: Springer, 2013.
42. Shilnikov, L. P., Shilnikov, A. L., Turaev, D., and Chua, L. O., *Methods of Qualitative Theory in Nonlinear Dynamics: Part 1*, World Sci. Ser. Nonlinear Sci. Ser. A Monogr. Treatises, vol. 4, River Edge, N.J.: World Sci., 1998.
43. Vitolo, R., Broer, H., and Simó, C., Routes to Chaos in the Hopf-Saddle-Node Bifurcation for Fixed Points of 3D-Diffeomorphisms, *Nonlinearity*, 2010, vol. 23, no. 8, pp. 1919–1947.
44. Vitolo, R., Broer, H., and Simó, C., Quasi-Periodic Bifurcations of Invariant Circles in Low-Dimensional Dissipative Dynamical Systems, *Regul. Chaotic Dyn.*, 2011, vol. 16, nos. 1–2, pp. 154–184.